frontiers | Frontiers in Earth Science

ORIGINAL RESEARCH
published: 01 June 2022
doi: 10.3389/feart.2022.857343

Characteristics of Lithofacies in Deep Shale Gas Reservoirs in the Southeast Sichuan Basin and Their Influence on Pore Structure

Jiang He[1], Songyue Zhu[1], Xuewen Shi[2], Shengxian Zhao[2], Lieyan Cao[2], Shulin Pan[1], Feng Wu[1] and Meng Wang[3,4]**

[1]School of Geoscience and Technology, Southwest Petroleum University, Chengdu, China, [2]Shale Gas Research Institute of PetroChina Southwest Oil and Gas Field Company, Chengdu, China, [3]School of Chemistry and Chemical Engineering, Chongqing University of Science & Technology, Chongqing, China, [4]Key Laboratory of Shale Gas Exploration, Ministry of Natural Resources, Chongqing Institute of Geology and Mineral Resources, Chongqing, China

The characteristics of lithofacies in the shale reservoir of the Wufeng and Longmaxi formations located in the Luzhou gas field were studied using the three-end-member method (mineralogical components). In addition, the microscopic characteristics and pore genesis of different lithofacies were studied and compared using TOC, FESEM, and digital core images. The results of the present study showed the development of five lithofacies: 1) quartz-rich argillaceous shale; 2) quartz/clay-mixed shale; 3) calcareous/clay-mixed shale; 4) calcium-rich argillaceous shale; and 5) clay-rich siliceous shale. The degree of pore development between lithofacies was highly heterogeneous. In addition, data indicated that total shale porosity increased with the increase in TOC. Thus, the pores were mainly related to organic matter. The enrichment of framboidal pyrite in quartz-rich shale (S1, S-3) and mixed shale facies (M-2, M-3) is essential during the formation of high-quality reservoirs. On the other hand, the content of organic matter in clayey shale was low, which does not favor the development of high-quality reservoirs. The differences in lithofacies pore structures are controlled by the sedimentary environment. The strong retention and reduction environment are the most favorable features for the formation of organic-rich siliceous shale lithofacies, which promote the preservation of organic matter and the development of reservoirs.

Keywords: shale, lithofacies, Ordovician Wufeng formation, Silurian Longmaxi formation, Luzhou field, Sichuan Basin

OPEN ACCESS

Edited by:
Shuai Yin,
Xi'an Shiyou University, China

Reviewed by:
Bo Jiu,
China University of Geosciences, China
Weiming Wang,
China University of Petroleum, China

****Correspondence:***
Jiang He
hejiang_swpu@126.com
Meng Wang
wangmeng_cqust@126.com

Specialty section:
This article was submitted to Economic Geology, a section of the journal Frontiers in Earth Science

Received: *19 January 2022*
Accepted: *21 April 2022*
Published: *01 June 2022*

Citation:
He J, Zhu S, Shi X, Zhao S, Cao L, Pan S, Wu F and Wang M (2022) Characteristics of Lithofacies in Deep Shale Gas Reservoirs in the Southeast Sichuan Basin and Their Influence on Pore Structure. Front. Earth Sci. 10:857343. doi: 10.3389/feart.2022.857343

1 INTRODUCTION

Shale gas resources play an important role in the world energy supply (Dong et al., 2011). With the development of unconventional oil and gas exploration and production, the study of shale pore structure has attracted extensive attention (Zou et al., 2010; Zou et al., 2015). As a result of commercial development of shale gas in North America, differences in mineralogical composition, gas-bearing storage, and compressibility of several lithofacies have been documented (Abouelresh and Slatt, 2012). These variations indicate that potential development of the lithofacies will also be different. The marine shale of the Wufeng and

Longmaxi formations in the Sichuan Basin is an important shale gas exploration and development succession in China. Its lithofacies division and the genesis of high-quality reservoir intervals have attracted significant attention (Chen et al., 2015; Zhao et al., 2016).

Lithofacies is a component of sedimentary facies. The study of lithofacies is essential during shale reservoir characterization and shale oil and gas reservoir evaluation (Wang and Carr, 2012). Shale lithofacies types are divided according to their characteristics using petrological, geochemical, and geophysical methods, which consider mineral composition, paleontology, structural strength, mineral content, and distribution. Among them, the most widely used method includes the three-end elements: clay minerals; carbonate rocks; and quartz and feldspar (Allix et al., 2010). The proper characterization of shale lithofacies includes the relationship between micropore structure and macro-sedimentary facies, mineral structure, and reservoir characteristics, as well as gas bearing and geomechanical properties of the reservoir. This information is extremely helpful for decision-making purposes during exploration and production of shale gas.

Considering different factors including climate change, material supply, and sea-level change, among others, different lithofacies are subjected to dissimilar sedimentary environments. For this reason, their mineral composition, organic matter content, and sedimentary structure display variability. In general, the shale reservoirs present low porosity and ultra-low permeability, as well as various pore types and wide pore size distribution, which results from an extremely complex pore structure (Liu et al., 2022). Different types of pore bodies are formed in different diagenetic stages and have various genetic types. Sedimentation, structure, and diagenetic evolution have an important impact on the evolution, preservation, and buried depth of shale reservoirs. These features determine the temporal and spatial distribution of high-quality shale reservoirs (Li et al., 2019; Li et al., 2020). Marine shale is highly heterogeneous. Different lithofacies display significant differences in pore structures. In silica shale, the degree of organic matter filling intergranular pores on large-scale is high. The clayey shale is affected by TOC content and organic matter clay complex structure. Organic pores present a wide pore size distribution, with a high average pore size; however, the total amount of organic pores is small (Fan et al., 2020). The organic pores are mainly developed in organic-rich shale facies of the shale gas reservoir. Several publications have reported on the influencing factors of organic matter abundance on the micropore structure. It has been found that organic carbon content determines the specific surface area and pore volume of micropores. In shales with elevated organic matter content, the higher the content of clay minerals, the higher the proportion of macropores (Li et al., 2019). This mainly occurs because of the large number of interlayer pores of nano-clay minerals, which promote the development of macropores.

Luzhou shale gas field, which formed in the southeast of the Sichuan Basin during the deposition of the first member of the Wufeng formation, can be divided into two parts: 1) shallow and 2) deep-water shelf parts (Ma et al., 2020). Since this is a new shale gas exploration block, little is known about its shale lithofacies and pore space characteristics. In addition, the control of lithofacies on reservoir pore type and the genetic mechanism of high-quality shale gas reservoirs is not clear. This restricts the evaluation and prediction of high-quality shale gas strata (Wang et al., 2017). For this reason, in order to provide a proper guidance for shale gas production, in the present study, we analyzed the relationship between shale lithofacies characteristics and pore type and structure.

2 SAMPLING AND METHODS

A total of 270 core samples were collected from 5 wells in the Lu203 well block located in the Wufeng and Longmaxi formations at depths between 3,892 m and 4051.15 m.

First, the rock type, mineralogical composition, particle shape, size and quantity, morphology, and size of pores and microcracks of 270 shale thin sections were analyzed using an Axioskop 40 polarizing microscope and FEI QUANTA 250 field emission scanning electron microscope (FESEM). PerGeos software was used to extract and segment pores from the images obtained by SEM, and the pore size and distribution characteristics of shale samples were quantitatively evaluated. In order to determine the mineralogical composition and lithofacies change in the vertical direction, the mineralogical composition and clay mineral type and content of 120 samples were quantitatively tested by using a PanalyticalX'Pert PRO MPD X-ray diffractometer, and the shale lithofacies types were classified according to the quantitative analysis results.

The total organic carbon (TOC) of 150 samples was analyzed using a LECO CS-200 carbon/sulfur analyzer to evaluate hydrocarbon generation potential. The plunger core porosity tester and STL—II high pressure permeability tester were used to determine the porosity and permeability of 140 core plug samples.

3 RESULTS

3.1 Mineralogical Composition of Shale

The X-ray diffraction results showed that the main mineral components were quartz, feldspar, calcite, dolomite, pyrite, and clay. The content of quartz and clay minerals accounted for more than 60% of the total, and the clay minerals consisted of illite, a mixed layer of illite/montmorillonite, and chlorite–kaolinite. The content of brittle minerals was between 31.8 and 97.0%, with an average of 64.1%, and a median of 62.0%. In addition, the content of clay minerals was 3.0%–59%, with an average of 29.5%, and a median of 28.0% (**Figure 1**).

The analysis of 256 samples from the Wufeng and Longmaxi formations showed a TOC between 0.1% and 9.3%, with an average of 2.1%. Among them, the TOC of gas reservoir samples was between 1.1% and 9.3%, with an average value of 2.9%. TOC varied between 2.0% and 4.0%, accounting for 63% of the total. According to the microscopic examination of kerogen in the core samples of Longmaxi formation, the average content of the sapropel group was more than 90%. The organic matter of the Wufeng and Longmaxi formations' organic-rich shale was mainly of type I kerogen.

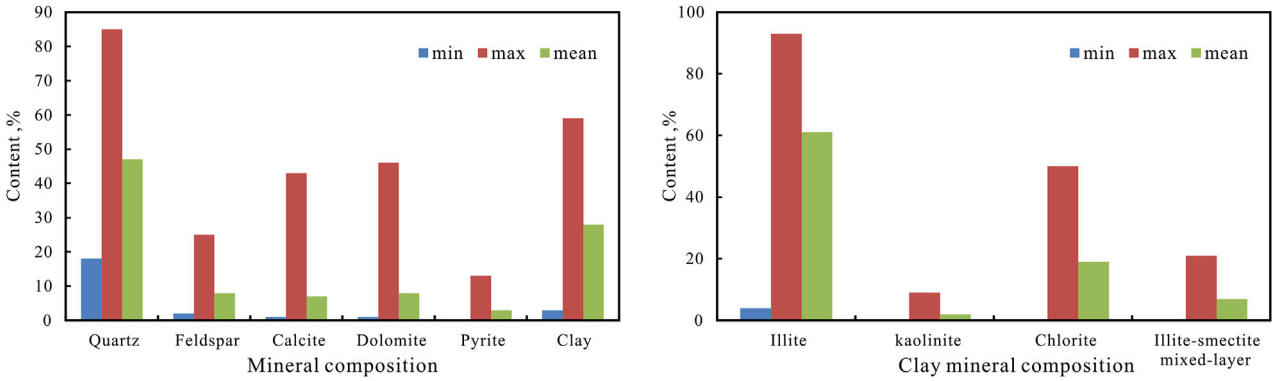

FIGURE 1 | Mineral composition histogram of the shale reservoir; **(A)** mineral composition and **(B)** clay mineral composition. min: minimum content value; max : maximum content value; mean: mean content value.

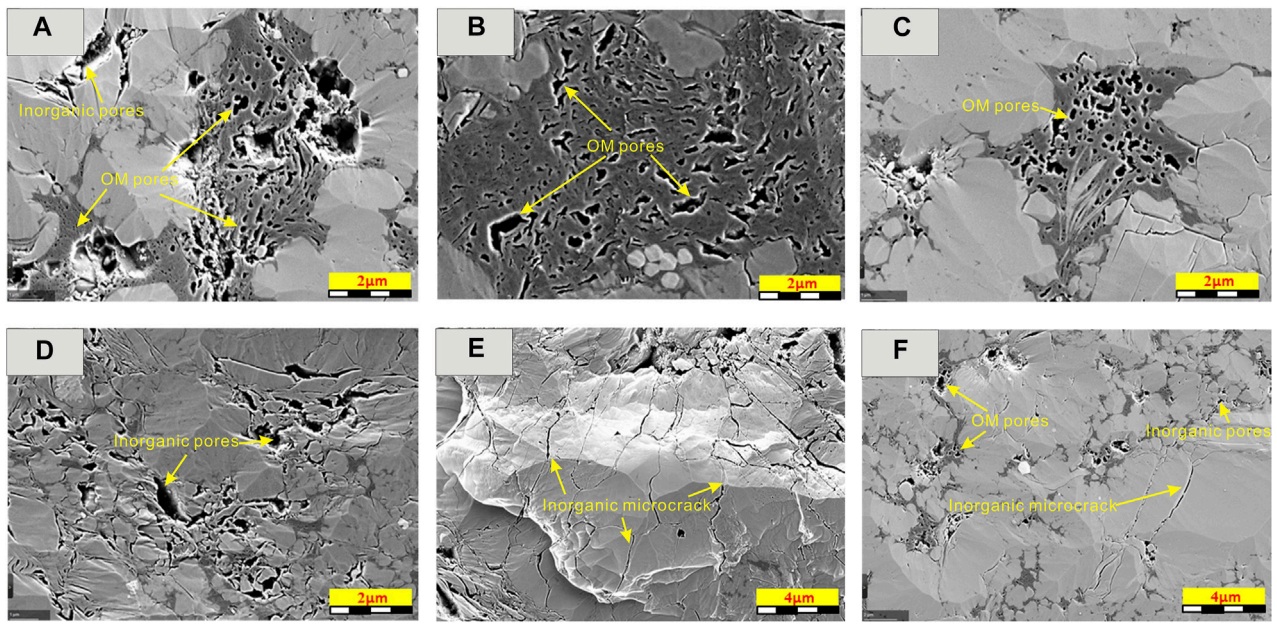

FIGURE 2 | Photographs of scanning electron microscopy (SEM) of the Wufeng–Longmaxi Formation shale; **(A)** inorganic pores and organic matter pores from L203 well, **(B)** organic matter pores from L205 well, **(C)** organic matter pores from L207well, **(D)** inorganic pores from L209 well, **(E)** inorganic microcrack from L206 well, and **(F)** inorganic pores, microcracks, and organic matter pores from L208 well.

3.2 Shale Gas Reservoir Characteristics

3.2.1 Types and Characteristics of Pore Spaces

According to the SEM and composition results, the shale pores in the study area can be divided into four basic types: organic pores (**Figures 2A–C**), organic cracks, inorganic pores (**Figures 2D,F**), and inorganic cracks (**Figures 2E,F**). Among them, the organic pores are subdivided into two subclasses: organic matter evolution pores (intra-OM pores) and pores between organic matter. The organic cracks can be divided into two subclasses: internal cracks in organic matter and cracks between organic matter. In addition, the inorganic pores are subdivided into two subclasses: mineral intragranular pores and mineral intercrystalline pores. Also, the inorganic cracks are divided into inorganic cracks and mineral grain boundary cracks. The organic and inorganic pores represent the main reservoir spaces. The organic matter pores generally exist in the form of bubbles and pores, and the primary organic matter pores are less developed.

3.2.2 Physical Properties of the Shale Reservoir

According to the analysis of 140 core samples from the shale gas interval of the L203 block, the porosity varied between 2.19% and 5.65%, with an average of 3.74%, and a median of 3.79%. Among them, the samples with porosity of 2%–4% are generally typified as low-porosity reservoirs, which in the present study accounted for 57.9% of the total. According to the analysis of 77 samples

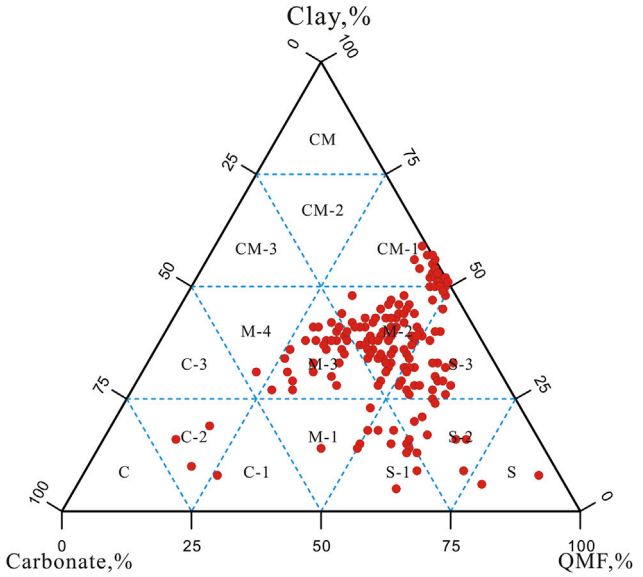

FIGURE 3 | Ternary lithofacies diagram of the Wufeng–Longmaxi Formation in the L203 well area SE Sichuan Basin. CM, mudstone facies; CM-1, silicon-rich argillaceous shale facies; CM-2, mixed argillaceous shale facies; and CM-3, calcium-rich argillaceous shale facies; S, siliceous facies; S-1, calcium-rich argillaceous shale facies; S-2, mixed siliceous shale facies; and S-3, mud-rich siliceous shale facies; C, limestone facies; C-1, silica-rich calcareous shale facies; C-2, mixed calcareous shale facies; and C-3, mud-rich calcareous shale facies; and M-1, calcareous/silica-mixed shale facies; M-2, silica/mud-mixed shale facies; M-3, calcareous/mud-mixed shale facies; and M-4, mixed shale.

from shale gas intervals of 2 wells, the matrix permeability varied between 3.98×10^{-5} mD and 9.81×10^{-2} mD, with an average of 1.12×10^{-2} mD. Thus, data indicated the presence of an ultra-low permeability reservoir.

The grain density of shale samples of different lithofacies varied from 2.4 g/cm^3 to 2.67 g/cm^3.

3.3 Lithofacies Division and Comparison of Shale Characteristics

The mineralogical composition measured by X-diffraction showed that this shale is mainly composed of quartz and clay minerals, with a small amount of carbonate minerals, feldspar, and pyrite. According to the division scheme proposed by Allix, the main types of lithofacies are divided by the relative contents of quartz, feldspar, clay minerals, and carbonate minerals (**Figure 3**).

The Wufeng and Longmaxi shale in the study area generally contains less than 50% clay and 25%–50% silica. Five types of lithofacies developed including silicon/mud mixed shale (M-2), calcareous/mud mixed shale (M-3), quartz-rich argillaceous shale (CM-1), mud-rich siliceous shale (S-3), and calcium-rich argillaceous shale (S-1) (**Figure 4**). Because of the high shale content, CM-1, M-2, and S-3 lithofacies reflect long-term stable sedimentation. Thus, they can be used as the unique lithofacies in deep-water sedimentary environments. M-3 represents the main shallow-water shelf lithofacies. In addition, S-1 corresponds to the common lithofacies in shallow-deep water sedimentary environments.

Clayey shales mostly contain clay mineral interlayer pores, intercrystalline pores, and organic matter pores, as well as a low content of organic matter. On the other hand, mixed shales display a high content of calcite and dolomite. In addition, the edge-dissolved pores and intercrystalline-dissolved pores of calcite and dolomite are relatively developed, with larger pore sizes as compared to those observed in the organic matter pores and clay intercrystalline pores. Moreover, most of the dissolution pores are filled with migrating organic matter (Wang et al., 2018). The sedimentary environment of siliceous shale presents an anoxic deep-water environment. In this case, pyrite is relatively developed, and the intercrystalline pores of framboidal pyrite aggregates are almost filled with migrating organic matter (Loucks and Ruppel, 2007).

4 DISCUSSION

4.1 Genetic Mechanism of Shale Lithofacies

Dissimilar sedimentary environments result in differences in lithofacies. With respect to shale lithofacies, different mineral compositions, organic matter content, and sedimentary structures formed in various sedimentary environments result in different types of rocks.

Vertically, the Wufeng Formation of the Upper Ordovician developed a medium carbon siliceous shale with high carbonate content. Data indicated that a thin-layer of pyrite was developed along the bedding surface of the shale.

The sedimentary period of the lower member of the Longmaxi formation corresponds to a stagnant deep-water sedimentary environment, which developed a siliceous shelf. The shale facies correspond to thin-layer mixed shale and thick siliceous shale, with high organic carbon content.

During the sedimentary period of the middle Longmaxi formation, the water depth decreased, the sedimentary facies mostly corresponded to mixed and sandy shelf, the shale lithofacies were comprised of thin and mixed shale, and the organic carbon content displayed a medium level.

Moreover, the water depth of the upper member of the Longmaxi formation further decreased, and argillaceous shelves were mostly present in sedimentary lithofacies. In addition, thin-layer mixed shale and clayey shale formed the shale lithofacies, and a low organic carbon content was present.

From bottom to top, the content of organic matter and quartz gradually decreased, and the content of silt particles and clay gradually increased. In addition, sandy nodules and sandy strips were observed in the top core. Pyrite structures presented gradual transitions from thick-layered in the lower part to scattered-layered in the upper part. It was also observed that the input of terrigenous debris gradually increased from bottom to top, the hydrodynamic conditions gradually increased, the sedimentary water body decreased, and the characteristics of the sedimentary environment changed from strong retention and strong reduction to a weak reduction environment.

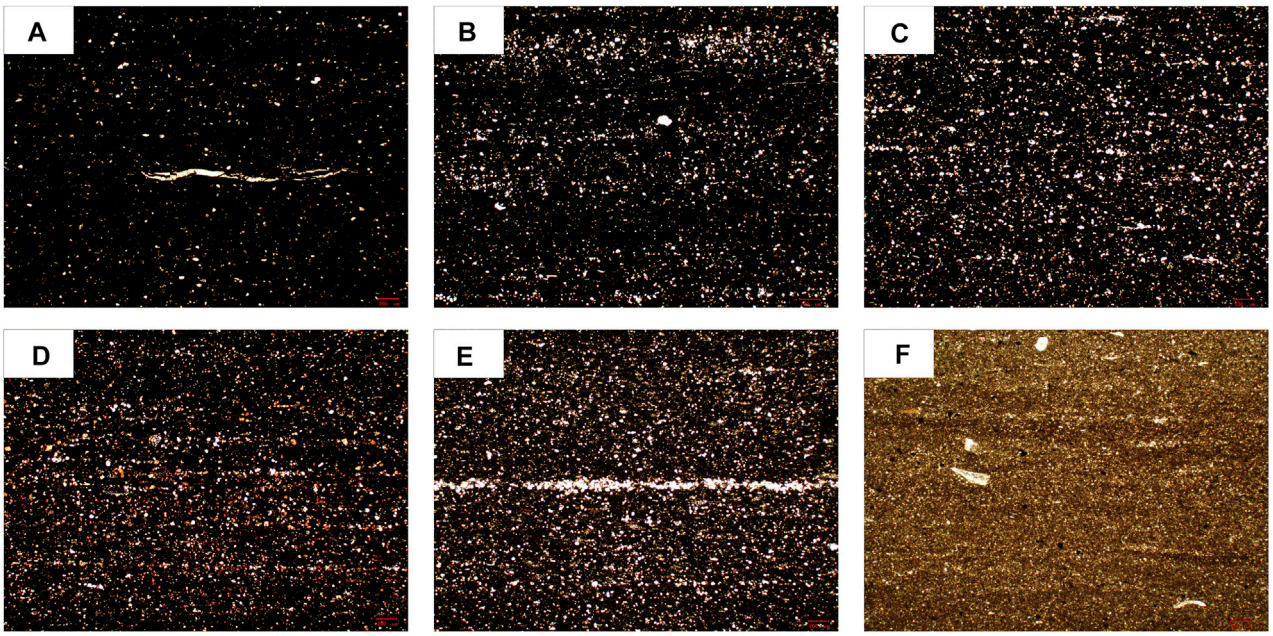

FIGURE 4 | Characteristics of shale of different lithofacies under polarizing microscope. **(A)** CM-1 lithofacies, 2983.78 m, well L205; **(B)**M-2 lithofacies, 4016.32 m, well L205; **(C)** M-3 lithofacies, 4026.12 m, well L205; **(D)**S-3 lithofacies, 4029.97 m, well L205; **(E)** S-2 lithofacies, 4032.58 m, well L205; and **(F)** S-1 lithofacies, 4041.67 m, well L205.

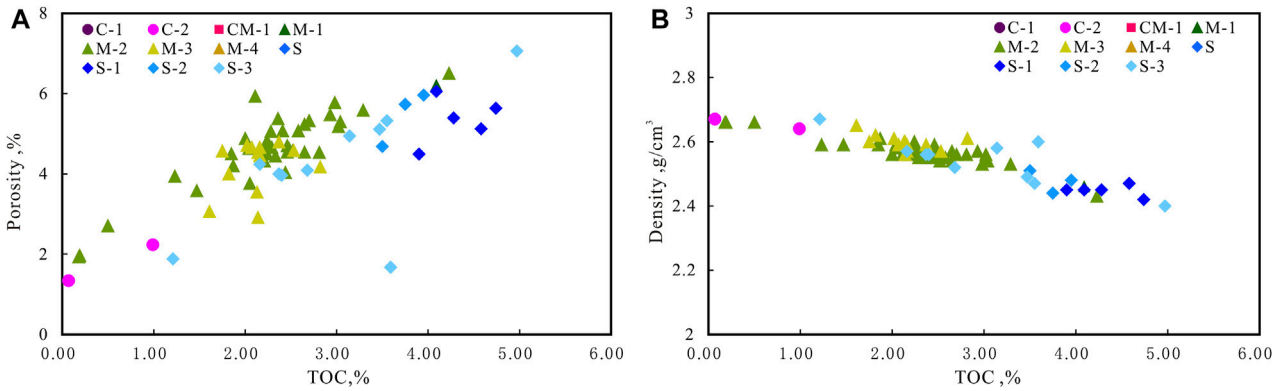

FIGURE 5 | TOC versus porosity **(A)** and density **(B)** of shale samples from Wufeng–Longmaxi Formation in the L203 well area.

With respect to the main shale facies, the mineral composition in the siliceous shale facies was relatively pure and contained pyrite. This indicated that the sedimentary environment was a relatively quiet and anoxic reduction environment. In the mixed siliceous shale facies, the clay minerals and carbonate mineral contents were less than 25%. In this case, foliation developed. It was also observed that micro-characteristic quartz was evenly distributed and scattered pyrite, and relatively developed silty laminae were distributed along the layers. These data indicated that a gradual change from an early strong reduction environment to a weak reduction environment occurred. In clay-bearing siliceous shale facies, clay mineral content increased. Silty strips as well as a progressive bedding development were observed in the core. This result suggested the enhanced supply of terrigenous debris and the transition of the sedimentary environment from a weak reduction environment to an oxidation environment.

4.2 Influence of Lithofacies on Organic Geochemical Characteristics

The enrichment of organic matter is usually related to the paleoenvironment (Xie et al., 2008). Generally, the anaerobic environment has a strong reduction ability, which promotes the preservation and enrichment of organic matter. The organic

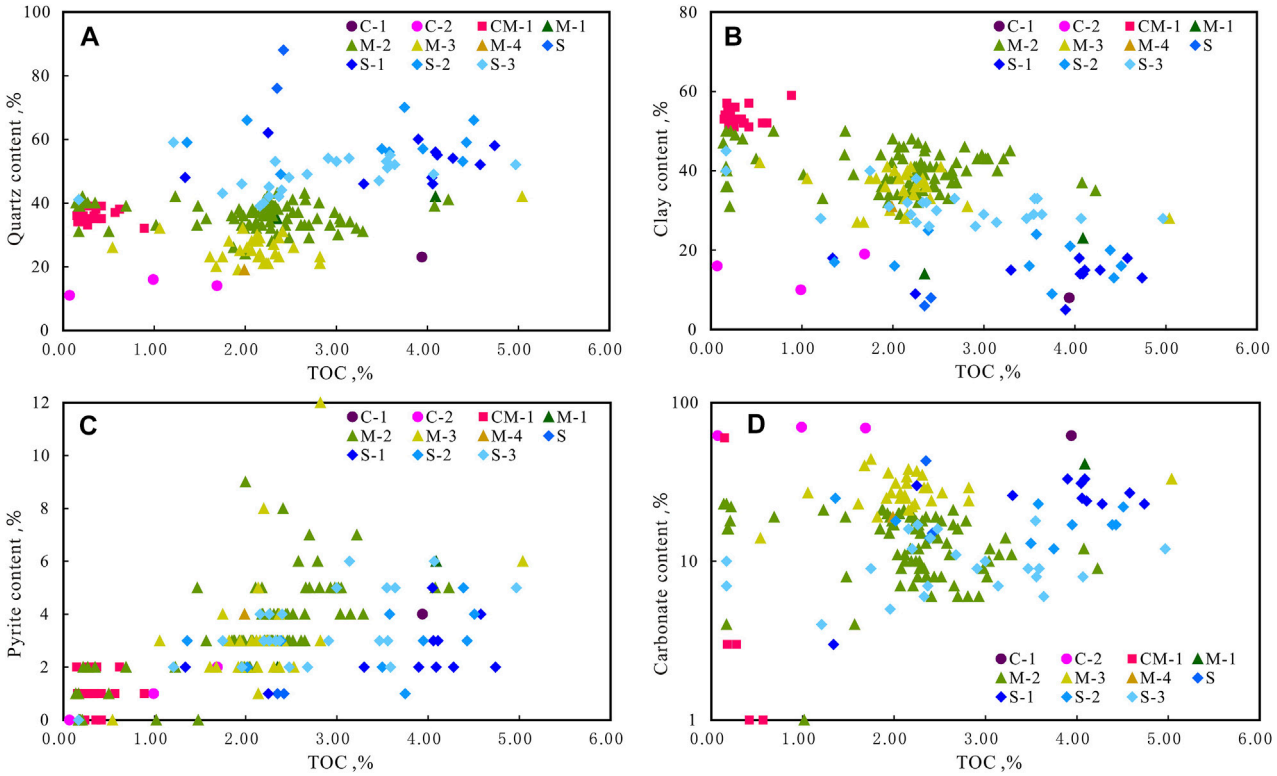

FIGURE 6 | TOC versus quartz content **(A)**, clay content **(B)**, pyrite content **(C)**, and carbonate content **(D)** of the shale samples from Wufeng–Longmaxi Formation in the L203 well area.

matter present in the deep shale reservoir significantly contributes to permeability, especially in the interval dominated by organic matter pores where the porosity is greatly affected by TOC. The results indicated good correlation coefficients between TOC-porosity and TOC-density, with values of 0.68 and 0.82, respectively (**Figure 5**). The highest TOC, porosity, and density correlations corresponded to those in mixed lithofacies. According to these results, the organic matter in mixed lithofacies is the main parameter controlling pore development. It was also observed that shale density decreased with the increase in TOC, and the total porosity increased with the increase in TOC. These data indicated that in the deep shale reservoir, organic matter pores were mostly present (Schlanser et al., 2016; Wang et al., 2018).

The relationship between clay minerals, quartz, and TOC content shows that TOC is positively correlated with quartz content (**Figure 6A**) but negatively correlated with clay mineral content (**Figure 6B**). These results indicated that siliceous shale was mainly derived from biogenic silicon, which also suggests that organic matter content in shale rich in clay minerals is relatively low. The relationship between pyrite, carbonate minerals, and TOC concentrations showed that TOC was positively correlated with pyrite content (**Figure 6C**) but not with carbonate mineral content (**Figure 6D**). Thus, pyrite influences the formation of organic pores to a certain extent (Wang et al., 2020).

The TOC in shale samples of main lithofacies varied from 0.07% to 5.04%. The data indicated that the siliceous shale displayed the highest TOC content. In the S-1 and S-3 shale facies, TOC varied from 1.36% to 4.97%, while in M-2 and M-3 facies, the TOC values were between 0.54% and 4.23%. The lowest TOC values were observed in CM-1 facies with numbers varying from 0.15% to 0.89%.

Clay shale displays high clay mineral content and low TOC content. Compared with mixed shale and siliceous shale, organic matter accounts for a relatively low proportion. The present study demonstrated that the development of organic matter pores controls the pore space of siliceous shale and mixed shale, while the pore space of clayey shale is mainly affected by the pore development of clay minerals. Quartz in siliceous shale mostly comes from the dissolution and reprecipitation of siliceous organisms such as radiolaria and siliceous sponges. Some pores between microcrystalline authigenic quartz particles provide a storage space for migrating organic matter. In addition, the bubble pores and sponge pores can be formed in organic matter. The TOC content in the mixed shale was slightly lower than that in siliceous shale and its micropores and mesopores were

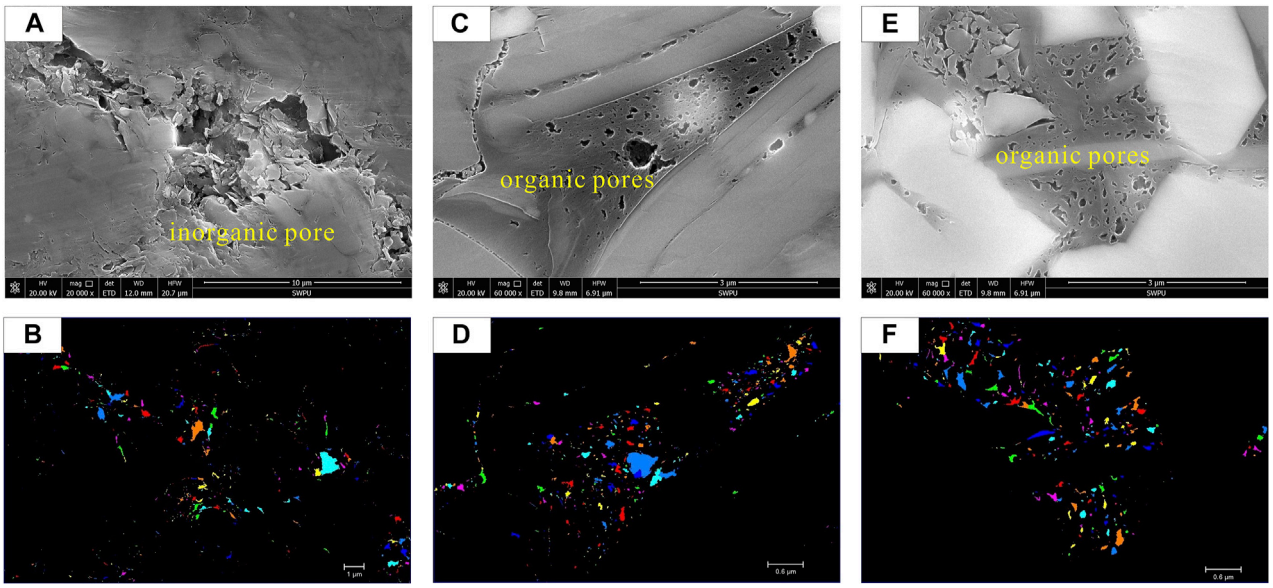

FIGURE 7 | Microphotographs showing main pore types and distribution characteristics of shale reservoir. **(A)** Inorganic pores, 3939.25 m, L206 well; **(B)** pore morphology and distribution of graph a; **(C)** organic pores and grain boundary pores, 3967.62 m, L206 well; **(D)** pore morphology and distribution of graph c; **(E)** pyrite intercrystalline pores and organic pores between pyrite crystals, 3980.96 m, L206 well; **(F)** pore morphology and distribution of graph **(E)**.

mostly composed of clay mineral-related pores, quartz intercrystalline pores, and organic matter pores. In addition, the increase in carbonate mineral content can provide dissolution pores for the preservation of migrating organic matter to a certain extent.

4.3 Origin of Different Pores in Deep Shale Reservoirs

Differences in the genesis of organic pores, inorganic pores, and inorganic cracks in the main spaces of deep shale reservoirs have been observed (Chen et al., 2015; Zhang et al., 2018).

Inorganic pores can be divided into intragranular and intercrystalline pores. The inorganic intragranular pores of black shale in the Luzhou area mainly developed in quartz, clay, feldspar, pyrite, and carbonate minerals. In addition, quartz grains contain primary pores. The transformation from montmorillonite to illite during the burial of clay minerals may also result in the formation of intragranular pores. Also, dissolution pores are easily formed in unstable minerals such as feldspar and carbonates. Intragranular dissolution pores exist in single-crystal pyrite or framboidal pyrite. On the other hand, intragranular pores mostly display spherical, grooved, or honeycomb morphologies. The pore sizes vary from tens of nanometers to tens of microns, and the connectivity is relatively poor (**Figure 7A**). Shale intercrystalline pores are mainly formed by mutual support of the same or multiple minerals. Interparticle pores are formed between grains or crystals such as quartz, clay minerals, feldspar, and dolomite in which pore size is larger than that of intragranular pores.

The inorganic pores developed in shales where an abundance of organic matter is relatively low. They present smooth edges, oval shape, uniform individual size, and relatively large pore diameter. On the other hand, the organic pores develop in relatively high organic matter shales, display irregular edges, mostly flat shapes, as well as certain directionality and relatively small pore diameter. The organic pores are formed during hydrocarbon maturation. The organic pores are mostly found in gas generation window (RO > 1.2%), and a few of them are also observed in oil generation windows (RO between 0.6% and 1.0%) (Jarvie et al., 2007; Mastalerz et al., 2013). The black shale from the Wufeng and Longmaxi formations has reached the mature stage. Thus, kerogen and early oil pyrolysis asphalt will produce organic matter evolution pores (Zhao et al., 2016). During thermal evolution, kerogen is often mixed with clay, quartz, feldspar, carbonate, and other minerals to form spherical or porous honeycomb structures. The most common honeycomb-shaped organic pores are formed in mixtures of quartz and clay minerals (**Figures 7C,E**).

The shales contain different types of pores, which are mostly developed in organic matter, brittle minerals, and clay minerals, among others. Organic matter pores represent the main type of pore space. They are formed in organic siliceous shales and organic mixed shale lithofacies (Tang et al., 2015; Wang et al., 2016; Li, 2022). The organic matter pores in organic-rich siliceous shales are highly developed and present a nearly circular shape, good connectivity, and a pore diameter higher than 150 nm. Medium to high organic siliceous shales contain microcracks at the edge of organic matter and rigid minerals and dissolution pores in the rigid particles. The pores in organic matter are developed and present a small pore size and slightly poor connectivity. The organic matter-rich mixed shales show low organic matter content, intergranular pores, and locally developed microfractures.

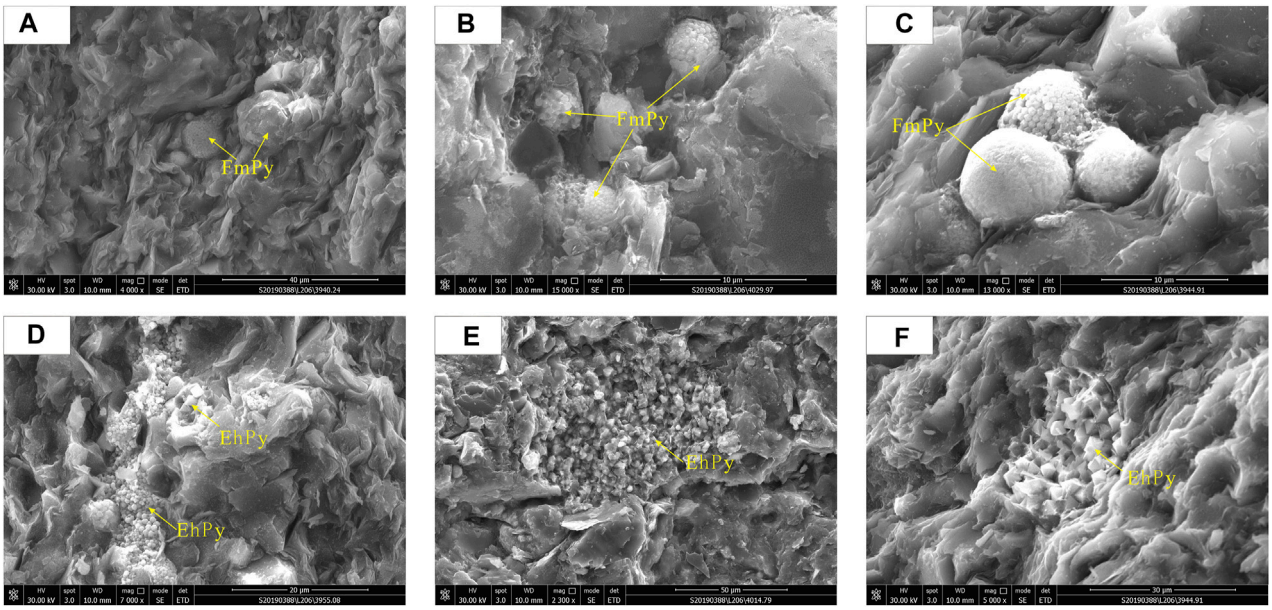

FIGURE 8 | Microphotographs showing different types of pyrites. **(A)** Framboidal pyrite (FmPy) associated with illite, 3940.24 m, L206; **(B)** framboidal pyrite (FmPy), 4029.97 m, L206; **(C)** framboidal pyrite (FmPy), 3944.96 m, L206; **(D)** lamellar euhedral pyrite aggregate (EhPy), 3955.08 m, L206; **(E)** euhedral pyrite aggregate (EhPy), 4014.79 m, L206; and **(F)** euhedral pyrite (EhPy), 3944.96 m, L206.

Gas-bearing property is an important index to measure the productivity of shale reservoirs. Organic matter is the material source of shale gas. In the process of hydrocarbon generation by organic matter, high-pressure protective pores and organic pores are formed. The higher the organic carbon content and the larger the total volume of micropores, the larger the surface area available for adsorption of adsorbed gas. Thus, total gas content increases (Hubbert, 1953; England et al., 1987). TOC presents a positive correlation with total gas content and porosity. Among siliceous shales, high carbon siliceous shales are the ones with the highest content of gas, which is usually more than 6.5 cm^3/g, followed by medium carbon siliceous shale, with a gas content of 4.2 cm^3/g. The organic matter content of low-carbon siliceous shales is similar to that found in mixed shales. Because of the large difference in porosity, the gas content in low-carbon siliceous shales is higher than that of mixed shale. However, in both cases, the values are lower than 4.0 cm^3/g.

4.4 Influence of Pyrite on the Formation of High-Quality Reservoirs

Figure 8 indicated the presence of many types of framboidal, lamellar, and nodular pyrite in the study area (**Figure 8**). In addition, it was found that framboidal pyrite is composed of microcrystals (**Figures 8A–C**), which are generally polygonal, octahedral, or cubic with uniform sizes. Nodular pyrite is mostly distributed on the sedimentary surface of the laminated shale in the form of cubic euhedral single crystals. If these crystals are enriched to a certain extent, they will show fine macroscopical strips produced along the layer (**Figure 8D**). Euhedral pyrite exists in octahedral, cubic, and spherical shapes (**Figures 8E,F**). This type usually appears as isolated and aggregated particles, often as euhedral or semi-euhedral crystals with large variations in particle size. Euhedral pyrite usually coexists with clay particles or clay lamellae, in which the pyrite particles between clay lamellae are usually surrounded by organic matter. In general, heteromorphic pyrite does not present regular shapes. Compared with framboidal pyrite, heteromorphic crystals and aggregates of pyrite are usually irregular monomer particles or irregular aggregates.

Framboidal pyrites with high organic matter content reflects the reduction conditions of stable water bodies. In the study area, the increased pyrite content was accompanied by an increase in organic matter content. High-quality shales with high organic carbon content are also formed under this sedimentary condition. Pyrite is an indicator of organic matter content in a shale, which is consistent with the positive correlation between pyrite content and TOC (**Figure 6C**).

Shale pore type and pore structure directly affect the adsorption and flow capacity of shale gas. Pyrite structures present various pore types. Microcrystalline and intercrystalline pores are developed in the raspberry-like pyrite aggregates with the highest content in the shale (**Figure 9A**). At the same time, the special shape of raspberry-like pyrite crystals causes most of the voids between the internal grains to be filled with organic matter to form an organic/pyrite complex. In addition, a great number of organic matter pores are developed in the organic matter structure (**Figure 9B**). Microscopic observations have shown that most organic

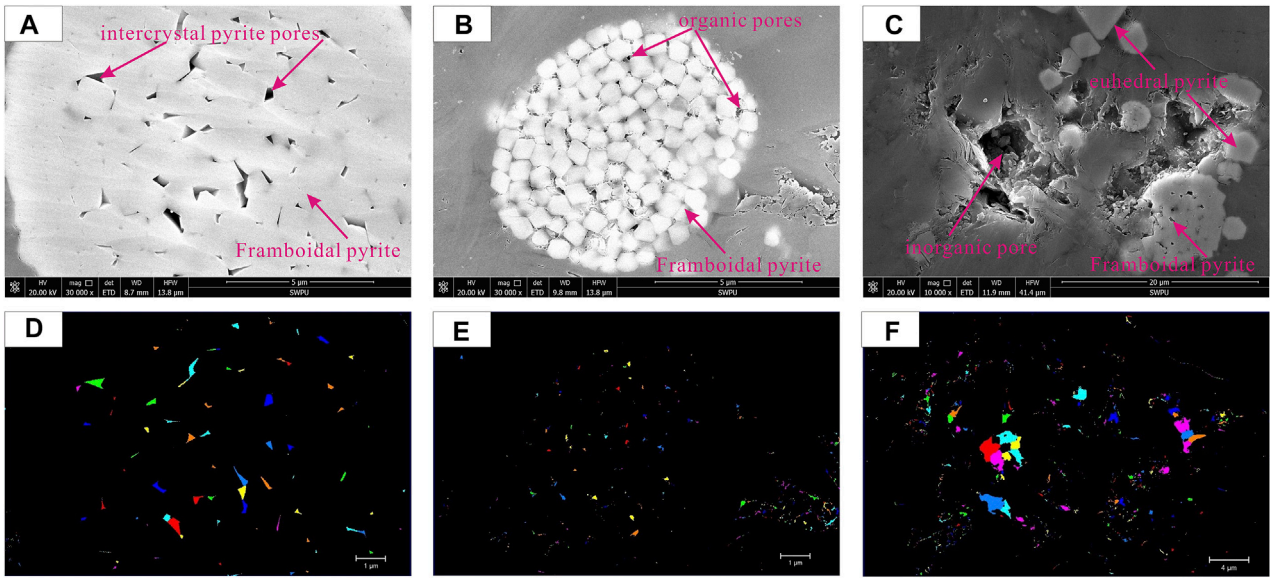

FIGURE 9 | Microphotographs showing pyrite and micropore development characteristics. **(A)** Intercrystal pyrite pores are developed in framboidal pyrite (FmPy), 3786.85 m, L208 well; **(B)** intercrystal pyrite pores and organic pores are developed in framboidal pyrite, 3830.40 m, L208 well; **(C)** inorganic pores, euhedral pyrite, and framboidal pyrite, 3840.43 m, L208 well; **(D)** pore morphology and distribution of graph a; **(E)** pore morphology and distribution of graph b; **(F)** pore morphology and distribution of graph **(C)**

matter pores are irregular and develop between organic matter or around the grain edge. Due to the support and protection of pyrite aggregates and the role of catalytic organic matter in hydrocarbon and gas generation, the number of pores in pyrite is more than that in surrounding organic matter (Han and Li, 2019). In addition, some mold pores are formed by the effect of crystals falling off the surface of the aggregate (**Figure 9C**). The pore size is generally larger than that in the internal organic matter pore, and the shape depends on the morphology of exfoliated crystals, which mostly display honeycomb shapes. Since they contain large pore sizes, they represent the main enrichment site of free gas.

A significant amount of space for the storage of oil and gas is provided by intercrystalline pores present in framboidal pyrite and pores formed by intercrystalline pyrite filled with organic matter (Zhao et al., 2016; Han and Li, 2019; Wang et al., 2020). The high content of pyrite results in the development of high-quality reservoirs. Among various lithofacies, the highest pyrite content corresponds to that of siliceous shale (S-2 and S-3) and mixed shale (M-2 and M-1), with average values of more than 3.3%. The average pyrite content in M-3 facies is 2.9% and that in other lithofacies is less than 2%.

The shale in the study area was divided into three categories: siliceous shale, calcareous shale, and mixed shale. Comparing different lithofacies, the type and content of pyrite are quite different. The highest pyrite content was found in the mixed shale, where pyrite was distributed in strips. The second highest pyrite content was determined in siliceous shale, which was scattered along the layer. Finally, the smallest amounts of pyrite were found in the calcareous shale. Our results were consistent with those reported in previous studies (Wu et al., 2016). The supporting framework composed of quartz in the shale provides a good space for kerogen preservation. The development of clay minerals has a catalytic effect on kerogen. Pyrite was mainly found in strawberry-like structures and irregular non-idiomorphic arrangements.

The time framework for the formation of pyrite is the same as that of early diagenetic formation. Pyrite, one of the common minerals present in shale reservoirs, plays a certain role in controlling the enrichment and production of shale gas.

Three different types of organic pores developed in organic matter migrate into pyrite minerals: 1) pyrite is associated and developed next to the migrated organic matter, and the formation period of pyrite occurs earlier with respect to that of organic matter. Pyrite plays a catalytic role in the formation of organic pores. 2) The transported organic matter fills the spaces between pyrite particles, and organic matter pores develop. Similar single-grain sizes and shapes of pyrite are formed in the same period, and some single crystals are formed in inorganic minerals. This occurs earlier with respect to the transport of organic matter. 3) The transported organic matter fills the spaces in pyrite particles, and organic matter pores develop. Pyrite obviously preceded the formation of organic matter.

The number and size of organic pores developed in the presence of pyrite are significantly better than those formed without pyrite. This indicates that pyrite has a very positive impact on the formation of organic pores. In the latter two types, pyrite not only catalyzes but also supports and protects organic pores. Most pyrite in shale exists in the form of strawberry-like pyrite structures. The best degree of pore development corresponds to the second type of organic pore.

5 CONCLUSION

1) The shale reservoir of the Wufeng and Longmaxi formations in the Luzhou block is characterized by low porosity and ultra-low permeability. Vertically, the development degree of organic pores and inorganic pores is highly heterogeneous. According to mineralogical composition, the main lithofacies in the study area were identified as quartz-rich argillaceous shale facies, silica/mud-mixed shale facies, calcareous/mud-mixed shale facies, calcium-rich argillaceous shale facies, and mud-rich siliceous shale facies.
2) Total shale porosity increases with the increase in TOC. In addition, in deep shale, mainly organic matter pores are present. Siliceous shale (S1 and S-3) and mixed shale (M-2 and M-3) contain a significant amount of intercrystalline pores in framboidal pyrite and pores generated by pyrite intergranular filling organic matter, which promote the formation of high-quality reservoirs. The pore space in clay shale is mainly affected by the organic pore development in clay minerals.
3) The differences in the sedimentary environment control the pore structure in lithofacies. The strong retention and reduction environment provide the conditions needed for the enrichment and preservation of organic matter. The organic-rich siliceous shale facies formed in this environment favor the formation of pores with large diameters in the organic matter structures. Thus, organic matter displays high porosity and gas content. In conclusion, organic-rich siliceous shale facies represent the most favorable lithofacies for the development of shale reservoirs.

DATA AVAILABILITY STATEMENT

The original contributions presented in the study are included in the article/Supplementary Material; further inquiries can be directed to the corresponding author.

AUTHOR CONTRIBUTIONS

JH contributed as the major author of the manuscript. SZ, XS, and SZ conceived the project. LC and SP collected the samples. FW and MW analyzed the samples. All authors contributed to the manuscript and approved the submitted version.

FUNDING

This study received support from the Science and Technology Cooperation Project of the CNPC-SWPU Innovation Alliance (2020CX020000), the China Postdoctoral Science Foundation (2017M623059), the General Project of Chongqing Natural Science Foundation (No.cstc2021jcyj-msxmX0897) the Major Scientific and Technological Project of Sichuan Province (2020YFSY0039), and the Opening Foundation of Key Laboratory of Shale Gas Exploration, Minisitry of Natural Resources (KLSGE-202102).

ACKNOWLEDGMENTS

We would like to thank reviewers for their suggestions.

REFERENCES

Abouelresh, M. O., and Slatt, R. M. (2012). Lithofacies and Sequence Stratigraphy of the Barnett Shale in East-Central Fort Worth Basin, Texas. *Bulletin* 96 (1), 1–22. doi:10.1306/04261110116

Allix, P., Burnham, A., Fowler, T., and Herron, M. (2010). Coaxing Oil from Shale. *Oilfield Rev.* 22 (4), 4–15.

Chen, L., Lu, Y., Jiang, S., Li, J., Guo, T., and Luo, C. (2015). Heterogeneity of the Lower Silurian Longmaxi Marine Shale in the Southeast Sichuan Basin of china. *Mar. Petroleum Geol.* 65, 232–246. doi:10.1016/j.marpetgeo.2015.04.003

Dong, D. Z., Zou, C. N., and Li, J. Z. (2011). Resource Potential, Exploration and Development Prospect of Shale Gas in the Whole World. *Geol. Bull. China* 30 (2), 324–336. doi:10.3969/j.issn.1671-2552.2001.02.18 (in Chinese with English abstract).

England, W. A., Mackenzie, A. S., Mann, D. M., and Quigley, T. M. (1987). The Movement and Entrapment of Petroleum Fluids in the Subsurface. *J. Geol. Soc.* 144 (2), 327–347. doi:10.1144/gsjgs.144.2.0327

Fan, C., Li, H., Qin, Q., He, S., and Zhong, C. (2020). Geological Conditions and Exploration Potential of Shale Gas Reservoir in Wufeng and Longmaxi Formation of Southeastern Sichuan Basin, China. *J. Petroleum Sci. Eng.* 191, 107138. doi:10.1016/j.petrol.2020.107138

Han, S., and Li, W. (2019). Study on the Genesis of Pyrite in the Longmaxi Formation Shale in the Upper Yangtze Area. *Nat. Gas. Geosci.* 30 (11), 1608–1618.

Hubbert, M. H. (1953). Entrapment under Hydrodynamic Conditions. *AAPG Bull.* 37 (8), 1954–2026. doi:10.1306/5ceadd61-16bb-11d7-8645000102c1865d

Jarvie, D. M., Hill, R. J., Ruble, T. E., and Pollastro, R. M. (2007). Unconventional Shale-Gas Systems: The Mississippian Barnett Shale of North-Central Texas as One Model for Thermogenic Shale-Gas Assessment. *Bulletin* 91 (4), 475–499. doi:10.1306/12190606068

Li, H., Qin, Q., Zhang, B., Ge, X., Hu, X., Fan, C., et al. (2020). Tectonic Fracture Formation and Distribution in Ultradeep Marine Carbonate Gas Reservoirs: A Case Study of the Maokou Formation in the Jiulongshan Gas Field, Sichuan Basin, Southwest China. *Energy fuels.* 34 (11), 14132–14146. doi:10.1021/acs.energyfuels.0c03327

Li, H. (2022). Research Progress on Evaluation Methods and Factors Influencing Shale Brittleness: A Review. *Energy Rep.* 8, 4344–4358. doi:10.1016/j.egyr.2022.03.120

Li, H., Tang, H., Qin, Q., Zhou, J., Qin, Z., Fan, C., et al. (2019). Characteristics, Formation Periods and Genetic Mechanisms of Tectonic Fractures in the Tight Gas Sandstones Reservoir: A Case Study of Xujiahe Formation in YB Area, Sichuan Basin, China. *J. Petroleum Sci. Eng.* 178, 723–735. doi:10.1016/j.petrol.2019.04.007

Liu, J., Yang, H., Xu, K., Wang, Z., Liu, X., Cui, L., et al. (2022). Genetic Mechanism of Transfer Zones in Rift Basins: Insights from Geomechanical Models. *GSA Bull.* doi:10.1130/B36151.1

Loucks, R. G., and Ruppel, S. C. (2007). Mississippian Barnett Shale: Lithofacies and Depositional Setting of a Deep-Water Shale-Gas Succession in the Fort Worth Basin, Texas. *Bulletin* 91 (4), 579–601. doi:10.1306/11020606059

Ma, X., Xie, J., Yong, R., and Zhu, Y. (2020). Geological Characteristics and High Production Control Factors of Shale Gas Reservoirs in Silurian Longmaxi Formation, Southern Sichuan Basin, SW China. *Petroleum Explor. Dev.* 47 (5), 841–855. doi:10.1016/s1876-3804(20)60105-7

Mastalerz, M., Schimmelmann, A., Drobniak, A., and Chen, Y. (2013). Porosity of Devonian and Mississippian New Albany Shale across a Maturation Gradient: Insights from Organic Petrology, Gas Adsorption, and Mercury Intrusion. *Bulletin* 97, 1621–1643. doi:10.1306/04011312194

Schlanser, K., Grana, D., and Campbell-Stone, E. (2016). Lithofacies Classification in the Marcellus Shale by Applying a Statistical Clustering Algorithm to Petrophysical and Elastic Well Logs. *Interpretation* 4 (2), E31–E49. doi:10.1190/int-2015-0128.1

Tang, X., Jiang, Z., Li, Z., Gao, Z., Bai, Y., Zhao, S., et al. (2015). The Effect of the Variation in Material Composition on the Heterogeneous Pore Structure of High-Maturity Shale of the Silurian Longmaxi Formation in the Southeastern Sichuan Basin, China. *J. Nat. Gas Sci. Eng.* 23, 464–473. doi:10.1016/j.jngse.2015.02.031

Wang, C., Zhang, B. Q., Lu, Y. C., Shu, Z. H., Lu, Y. Q., Bao, H. Y., et al. (2018). Lithofacies Distribution Characteristics and Main Development Controlling Factors of Shale in Wufeng Formation-Member 1 of Longmaxi Formation in Jiaoshiba Area. *Acta Pet. Sin.* 39 (6), 631–644. doi:10.7623/syxb201806003

Wang, G., and Carr, T. R. (2012). Methodology of Organic-Rich Shale Lithofacies Identification and Prediction: A Case Study from Marcellus Shale in the Appalachian Basin. *Comput. Geosciences* 49, 151–163. doi:10.1016/j.cageo.2012.07.011

Wang, M., Tang, H., Zhao, F., Liu, S., Yang, Y., Zhang, L., et al. (2017). Controlling Factor Analysis and Prediction of the Quality of Tight Sandstone Reservoirs: a Case Study of the He8 Member in the Eastern Sulige Gas Field, Ordos Basin, china. *J. Nat. Gas Sci. Eng.* 46, 680–698. doi:10.1016/j.jngse.2017.08.033

Wang, P., Jiang, Z., Ji, W., Zhang, C., Yuan, Y., Chen, L., et al. (2016). Heterogeneity of Intergranular, Intraparticle and Organic Pores in Longmaxi Shale in Sichuan Basin, South China: Evidence from SEM Digital Images and Fractal and Multifractal Geometries. *Mar. Petroleum Geol.* 72, 122–138. doi:10.1016/j.marpetgeo.2016.01.020

Wang, Z., Chen, L., Chen, D., Lai, J., Deng, G., Liu, Z., et al. (2020). Characterization and Evaluation of Shale Lithofacies within the Lowermost Longmaxi-Wufeng Formation in the Southeast Sichuan Basin. *J. Petroleum Sci. Eng.* 193 (1), 107353. doi:10.1016/j.petrol.2020.107353

Wu, L., Hu, D. F., Lu, Y. C., and Ruobing, L. I. U. (2016). Advantageous Shale Lithofacies of Wufeng Formation-Longmaxi Formation in Fuling Gas Field of Sichuan Basin, SW China. *Petroleum Explor. Dev.* 43 (2), 189–197. doi:10.1016/s1876-3804(16)30024-6

Xie, X. N., Li, H. J., Xiong, X., Huang, J., Yan, J., and Wu, L. (2008). Main Controlling Factors of Organic Matter Richness in a Permian Section of Guangyuan, Northeast Sichuan. *J. Earth Sci.* 19 (5), 507–517. doi:10.1016/s1002-0705(08)60056-4

Zhang, L., Lu, S., Jiang, S., Xiao, D., Chen, L., Liu, Y., et al. (2018). Effect of Shale Lithofacies on Pore Structure of the Wufeng-Longmaxi Shale in Southeast Chongqing, china. *Energy fuels.* 32, 6603–6618. doi:10.1021/acs.energyfuels.8b00799

Zhao, J., Jin, Z., Wen, X., Geng, Y., and Nie, H. (2016). Lithofacies Types and Sedimentary Environment of Shale in Wufeng-Longmaxi Formation, Sichuan Basin. *Acta Pet. Sin.* 37 (5), 572–586. doi:10.7623/syxb201605002

Zou, C., Dong, D., Wang, S., Li, J., Li, X., Wang, Y., et al. (2010). Geological Characteristics and Resource Potential of Shale Gas in China. *Petroleum Explor. Dev.* 37 (6), 641–653. doi:10.1016/s1876-3804(11)60001-3

Zou, C., Dong, D., Wang, Y., Li, X., Huang, J., Wang, S., et al. (2015). Shale Gas in China: Characteristics, Challenges and Prospects (I). *Petroleum Explor. Dev.* 42 (6), 753–767. doi:10.1016/s1876-3804(15)30072-0

Conflict of Interest: SX, ZS, and CL were employed by the Shale gas Research Institute of PetroChina Southwest Oil and Gas Field Company.

The remaining authors declare that the research was conducted in the absence of any commercial or financial relationships that could be construed as a potential conflict of interest.

Publisher's Note: All claims expressed in this article are solely those of the authors and do not necessarily represent those of their affiliated organizations, or those of the publisher, the editors and the reviewers. Any product that may be evaluated in this article, or claim that may be made by its manufacturer, is not guaranteed or endorsed by the publisher.

Copyright © 2022 He, Zhu, Shi, Zhao, Cao, Pan, Wu and Wang. This is an open-access article distributed under the terms of the Creative Commons Attribution License (CC BY). The use, distribution or reproduction in other forums is permitted, provided the original author(s) and the copyright owner(s) are credited and that the original publication in this journal is cited, in accordance with accepted academic practice. No use, distribution or reproduction is permitted which does not comply with these terms.